Cancer Management and Research

Dovepress
open access to scientific and medical research

Open Access Full Text Article

ORIGINAL RESEARCH

Improved ADM Penetration Distance and Therapeutic Efficiency in a Rabbit VX2 Liver Cancer Model by Relaxin Infusion Combined with Transcatheter Chemoembolization Through Hepatic Artery

This article was published in the following Dove Press journal:
Cancer Management and Research

Fu Xiong[1,2,*]
Yanyan Cao[1,2,*]
Xiaopeng Guo[1,2]
Hongsen Zhang[1,2]
Jihua Wang[1,2]
Bin Xiong[1,2]
Bin Liang[1,2]
Chuansheng Zheng[1,2]

[1]Department of Radiology, Union Hospital, Tongji Medical College, Huazhong University of Science and Technology, Wuhan, Hubei 430022, People's Republic of China; [2]Hubei Province Key Laboratory of Molecular Imaging, Wuhan, Hubei 430022, People's Republic of China

*These authors contributed equally to this work

Correspondence: Chuansheng Zheng
Email hqzcsxh@sina.com

Purpose: To evaluate the adriamycin (ADM) pervasion distance within tumor stroma after relaxin (RLX) infusion through tumor feeding artery and further investigate the therapeutic effects of RLX infusion combined with transcatheter chemoembolization (TACE) on the rabbit VX2 liver cancer, since the chemotherapy impaired due to limited drug distribution hindered by stiffened tumor stroma.

Materials and Methods: In the first part, rabbits received normal saline (NS), RLX or combined with TACE, and the penetration distance of ADM was measured by immunofluorescence and the matrix metalloproteinases (MMPs) were evaluated by gelatin substrate zymography in each group. In the second part, the rabbits received NS, TACE and RLX combined with TACE, respectively. The tumor growth rates, necrosis rates and intrahepatic metastasis were measured, and hematoxylin-eosin (HE), transferase-mediated dUTP-biotin nick end labelling (TUNEL) and Ki67 staining were conducted in each group.

Results: In the first part, the expression of MMP-9 was increased in groups treated by RLX compared with NS group, especially three days after RLX infusion ($p=0.001$). The ADM penetration distance was significantly increased in groups treated by RLX compared with NS group ($p<0.05$), and it was farthest three days after RLX infusion. In the second part, compared with the NS and TACE groups, the tumor growth rates, the positive staining rates of Ki67 and the tumor growth rates were significantly decreased in RLX+TACE group ($p<0.05$). However, the positive staining rates of TUNEL and the tumor necrosis rates were significantly increased ($p<0.05$), and HE staining also revealed higher necrosis rates. The intrahepatic metastasis indicates no difference between the three groups ($p=0.273$).

Conclusion: An increased penetration distance was obtained by RLX infusion through tumor feeding artery, and better therapeutic effects were achieved by RLX combined with TACE.

Keywords: relaxin, liver cancer, transcatheter chemoembolization, MMP-9, penetration distance

Introduction

Liver cancer is the sixth common tumor and the fourth leading cause of cancer death worldwide, and ranked as the second cause for the death of males.[1] However, there is no universally accepted satisfactory method for the treatment of liver cancer,

particularly in medium and advanced patients. Transcatheter chemoembolization (TACE), as a most frequently used first-recorded treatment in Asia and North America,[2] combines injection of chemotherapy with blockage of the tumor feeding artery which can result in extensive tumor necrosis and thus improve survival.[3–6] However, a clinical trial also demonstrated that the chemotherapy through transcatheter procedure has no significant effect compared with embolization alone.[7] The chemotherapy has been impaired because of the limited drug distribution hindered by stiffened extracellular matrix (ECM) within tumor.[8,9] This may provide some clue for improving efficiency by transcatheter chemotherapy through enhancing agent infiltration.

Tumor ECM, consisting of fibrous structural proteins (e.g., collagen and elastin), fibrous adhesive proteins (e.g., fibronectin and laminin) and proteoglycans,[10–12] forms the composition of stroma to interact with cancer cells and is immersed among them. The genes that restrain cell cycle progression could be inhibited by the adhesion of stiffened ECM, leading to promoted cancer cell growth.[13–15] Given that linearized fibers in ECM are stiffer than curly ones, so increasing ECM stiffness could provide "linear highway" which is observed in vivo by intravital imaging for malignant cells to move along, and speed up the migration of cancer cells in collagen-rich regions through integrins.[8,16,17] Besides promoting tumor progression, ECM also prevents intratumoral agent penetration because of the physical barrier created by dense stroma, thus it may mediate the resistance to chemotherapy.[8,18–20] Although TACE has been proved its efficacy in reducing interstitial fluid pressure and improving agent infiltration to some extent,[21,22] the biophysical features of the ECM can overwhelm its effect.

Human relaxin-2 (RLX), which has a similar structure to insulin, is a 6-kDa peptide hormone.[23] As a ligand for the RLX family peptide receptors 1 and 2, RLX is able to degrade stroma proteins by downregulation of ECM protein expression and upregulation of MMPs, such as MMP-2 and MMP-9.[9,24] What's interesting is that RLX predominantly decreases abnormally expressed ECM, fibrotic tissues and tumors for instance.[25] Furthermore, RLX has been used for degrading the tumor ECM components and achieving satisfactory outcomes in treating cancer when it is combined with trastuzumab or adenoviruses etc.[26–29]

Based on these researches, combining RLX with TACE procedure might be a promising therapeutic method to treat liver cancer, since the effect of transcatheter chemotherapy might be released richly while the RLX destroyed the physical ECM barrier after transcatheter procedure. In the present study, ADM was applied to identify that the drug penetration was improved through RLX transcatheter injection. Furthermore, the treatment effect was evaluated after combined use of RLX and TACE.

Materials and Methods

All facilities were approved by the Association for Assessment and Accreditation of Laboratory Animal Care. The VX2 tumor cells were reserved in our laboratory, adult New Zealand white rabbits (body weight, 2.5–3.0 kg) were purchased from the center of Experimental Animal of Huazhong University of Science and Technology. All VX2 tumor cells' and animal studies were approved by the Institutional Animal Care and Use Committee at Tongji Medical College, Huazhong University of Science and Technology, following the Guide for the Care and Use of Laboratory Animals published by the Chinese National Academy of Sciences.

Animal Model Establishment

The establishment of the rabbit VX2 hepatocellular carcinoma model was conducted as follows: first, the VX2 tumor cells were implanted into rear le.g.muscles of rabbits; second, the tumor was harvested from the carrier rabbit about 2 weeks after implanting, then minced into $1\times1\times1$ mm^3 and stored in normal saline; third, the abdominal median incision of the rabbit was conducted after general anesthesia by intravenous sodium pentobarbital (30 mg/kg body weight), and a fresh tumor fragment was inoculated into the left liver lobe, followed by gelatin tamping. Finally, the abdominal wall was sutured. Intramuscular injection of penicillin was given to the rabbits for three days after the operation above.

CT Scanning and Measurement of Tumor Characteristics

Dynamic contrast-enhanced CT of the rabbits was performed 2 weeks after implanting procedures, and 1 week after transcatheter procedures, respectively. The size and the appearance of the tumors were estimated applying the Syngo Fastview image processing system which was monitored by two senior doctors in the radiology field.

The volume of tumor was calculated according to the equation "$V=A\times B^2\times\pi/6$", therein A was recorded as the maximum diameter and B as the transverse diameter of the tumor. The tumor growth rate was calculated as "V2/V1", where V1 and V2 reflected pre-operation and post-operation volume of tumors, respectively. Furthermore, the necrosis rate was

calculated as "S2/S1", where S1 and S2 were referred to the area of tumor section and necrosis field, respectively. Moreover, S1 and S2 were both calculated as "S= c×d" measured by vernier caliper after harvesting tumor samples, where "c" and "d" referred to the maximum diameter and the transverse diameter of the tumor or its necrosis area, respectively. The intrahepatic metastasis of the rabbits was measured too.

Groups and Transcatheter Procedure

The rabbits were randomly assigned into nine groups (n=5 for each group): group 1 received normal saline (NS) through tumor feeding artery injection, combined with ADM (8mg/kg) which was delivered at the day of transcatheter procedures; rabbits in groups 2, 3, and 4 received RLX (5mg/mL, about 14μg in total, the same concentration into each rabbit) combined with ADM which was injected 1, 3 and 5 days after trancatheter procedures, respectively; rabbits in groups 5 and 6 received saline (3mL) and RLX, respectively, through tumor feeding artery, combined with ADM/Lipiodol emulsion (3mL) and gelfoam embolization (TACE); and those in groups 7, 8 and 9 received saline (3mL), TACE (3mL) and TACE (3mL) after RLX transcatheter injection, respectively.

The transcatheter procedure was performed one day after the CT scanning. Moreover, the rabbits were anesthetized in the same way as described above. Then the right femoral artery of rabbits was dissected bluntly, and an 18-gauge needle and a 4-Fr vascular sheath (Terumo, Tokyo, Japan) were utilized. A 4-Fr Cobra visceral catheter (Terumo) and a 2.7-Fr microcatheter (Terumo) were placed in the feeding arteries of the tumor by coaxial catheter technology under the guidance of digital subtraction angiography. Then different agents and saline were injected into the feeding artery of the rabbit as slow as possible.

Gelatin Substrate Zymography

All the rabbits were sacrificed by an overdose of chloral hydrate (10%) (Laboratory Animal Center, Huazhong University of Science and Technology). The tumor with surrounding liver tissues of rabbits in the groups 1, 2, 3 and 4 were harvested 4 hours later, after the injection of ADM. Afterwards, they were cut into two equal halves. One segment was for gelatin substrate zymography. Briefly, samples were loaded into an 8% zymogram gel copolymerized with 0.1% gelatin under nonreducing conditions. Then gels were washed twice with a 2.5% triton X-100 solution for 20 min, followed by a 20 min wash in incubation buffer (50mmol/L Tris-HCl (6.057g/L) tris base, 5mmol/L $CaCl_2$ (0.5549g/L), pH7.6). Zymograms were placed in fresh incubation buffer for 24 hours at 37°C. Then gels were stained with 0.05% Coomassie Brilliant Blue R-250 (Biossci, #BB0662, China) and destained in 10%, 10% and 5% destaining solution for 0.5, 1 and 2 hours, respectively, until the gelatinase (MMP-2, MMP-9) activity was clearly visualized as clear bands against a blue background. The gelatinase activity was analyzed according to the densitometry of bands by Quantity One software (Bio-Rad, Hercules, CA, USA).

Immunofluorescence

Immunofluorescence and image analysis were performed as described previously.[22] Briefly, in order to stain blood vessels, frozen sections of tissues were fixed in paraformaldehyde for 10 min, washed in Phosphate-buffered saline (PBS), and blocked with fetal calf serum (dilution, 1:20; Roche) for 20 min. Specimens were incubated overnight at 4°C with mouse anti-human CD31 monoclonal antibodies (dilution, 1:100; Dako), then washed in PBS and stained with goat anti-mouse secondary antibody Fitc (dilution, 1:50; Jackson) for 1 hour at room temperature. Then, DAPI nuclear dye was used to stain for 10 min. The doxorubicin auto-fluorescence and blood vessels were observed by a fluorescence microscope (Olympus, Tokyo, Japan) and captured by a camera (Q-IMAGING, British Columbia, Canada).

Microvessel density (MVD) was calculated by the method developed by Weidner et al.[30] First, the most intense vascularization of each tumor section was detected under a low magnification field (×40 magnification), then microvessels were counted at three high magnification fields (×100 magnification). The final MVD was the mean value of three fields. The calculation method of doxorubicin was similar to the method of MVD calculation. All these procedures were conducted by Image-Pro Plus 6.0 (Media Cybernetics, Rockville, MD, USA).

TUNEL and Ki67 Staining

TUNEL staining was performed as follows: Sections were routinely processed in 4% formamint first. Afterwards, they were rinsed twice with PBS for 10 min each time, and treated with 0.1% Triton X-100 in PBS for 2 min on ice. They were then rinsed in PBS again and incubated at 37 °C with 50 μL of TUNEL reaction solution for 60 min. After washing with PBS, the slides were analyzed by a fluorescence microscope (Olympus, Tokyo, Japan).

Ki67 staining was conducted through rinsing the sections with PBS. A monoclonal rabbit anti-Ki67 (Abcam, America) was used as a primary antibody for incubation overnight. Besides, a goat anti-rabbit IgG (Aspen, America) was used as a secondary antibody, which was incubated at 37 °C for 50 min after washing with PBS. Diaminobenzidine chromogenic Kit (ZSGB-BIO, Beijing, China) was used for detecting immunoreaction, which resulted in red color.

Statistical Analysis

Statistical analysis was performed by using SPSS software (SPSS, version 24.0, Chicago, IL, USA). Data were presented as means ± standard deviation. The measurement data were analyzed statistically by One-Way ANOVA. P<0.05 was considered as statistically significant. All the Figures were drawn by Graphpad prism V7.0 (GraphPad Software, San Diego, CA, USA).

Results

Tumor Size

The mean maximal diameters of tumors in groups 1, 2, 3 and 4 were 16.1±1.4 mm, 15.7±1.4 mm, 15.5±1.8 mm and 15.4 ±1.8 mm, respectively, and there was no significant difference among them (p=0.90). Moreover, there was no significant difference between the groups 5 and 6 in the mean maximal diameters (16.3±1.7 mm versus 16.7±1.5 mm) (p=0.85). Furthermore, the mean tumor diameters of groups 7, 8 and 9 were 17.0±1.8 mm, 17.7±2.7 mm and 16.0 ±3.5 mm, respectively, without significant difference (p=0.61) either.

MMP Activity

As shown in the Figure 1A, the MMP activities in groups 1 to 4 at different time points after transcatheter procedures were measured. There was significant difference between groups 1 and 3 (p=0.001) in the MMP activity at the 3rd day after RLX injection, which was evidently upregulated compared with the NS group. However, the difference of the MMP activities among other groups was not significant (p>0.05), while those at the 1st and 5th days after RLX transcatheter injection seemed more active than the NS group.

The MMP activity was further evaluated in groups 5 and 6, which underwent TACE after respective NS and RLX transcatheter injection. As shown in the Figure 1B, the MMP activity of the RLX combined with embolization group was significantly improved compared to the control group (p=0.008).

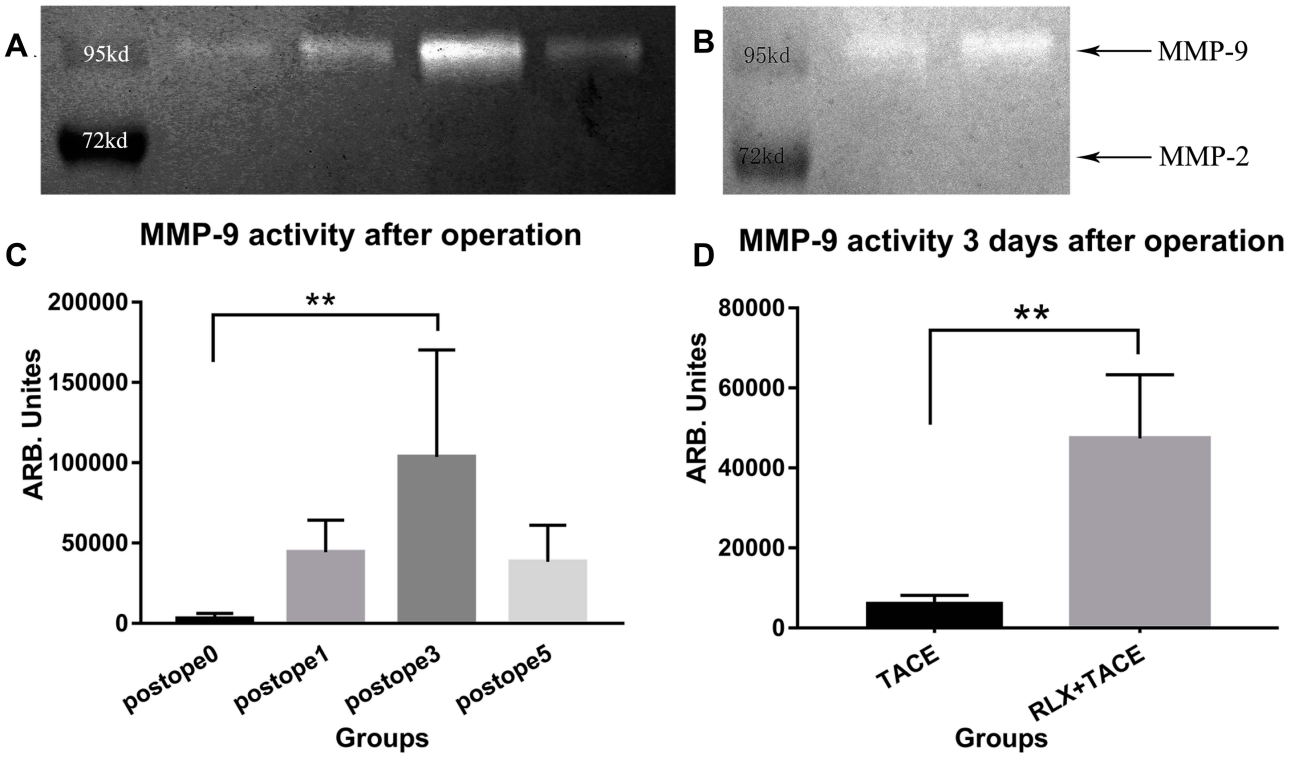

Figure 1 (**A–D**) Gelatin substrate zymography was employed to analyze the expression of MMP-2 and MMP-9 after RLX infusion in the first part of this study. Densitometry (each zymogram in the figure) was used to quantify band size as an indicator of relative MMP-9 activity. ** *P* <0.01.
Abbreviations: MMP, matrix metalloproteinase; RLX, relaxin.

Nevertheless, the MMP-2 activity was too low to be detected in these six groups (Figure 1).

ADM Distribution and MVD

The ADM auto-fluorescence was detected as red in the nuclei of cells. The ADM distribution distances of groups 1, 2, 3 and 4 were presented in the Figure 2A as well as the Figure 3A. The distribution distances of the groups were 71.64±3.59 μm, 124.70±15.37 μm, 241.56±35.75 μm and 151.66±20.23 μm, respectively. There was significant difference between groups 1 and 2 (p=0.002), 1 and 3 (p=0.000) as well as groups 1 and 4 (p=0.000), respectively. Compared with group 3, the difference was significant in groups 2 and 4 (p=0.000 and 0.000, respectively). However, the difference between groups 2 and 4 was not significant (p=0.071).

The ADM distribution distances of groups 5 and 6 were presented in the Figures 2B and 3B. The distribution distances

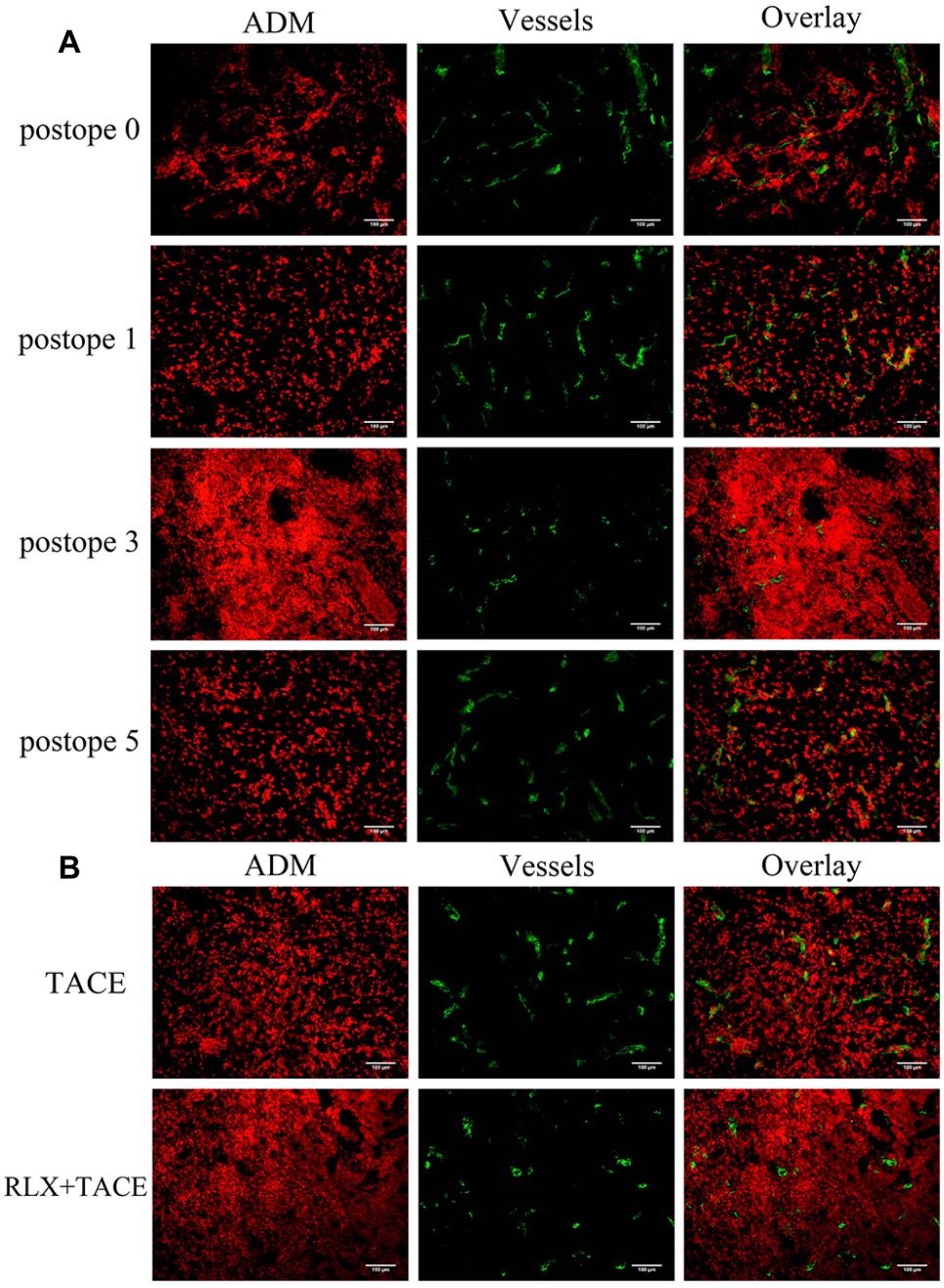

Figure 2 Immunofluorescence was performed for image analysis to evaluate the pervasion distance of ADM within the tumor stroma in group 1 to group 6.
Abbreviations: ADM, adriamycin.

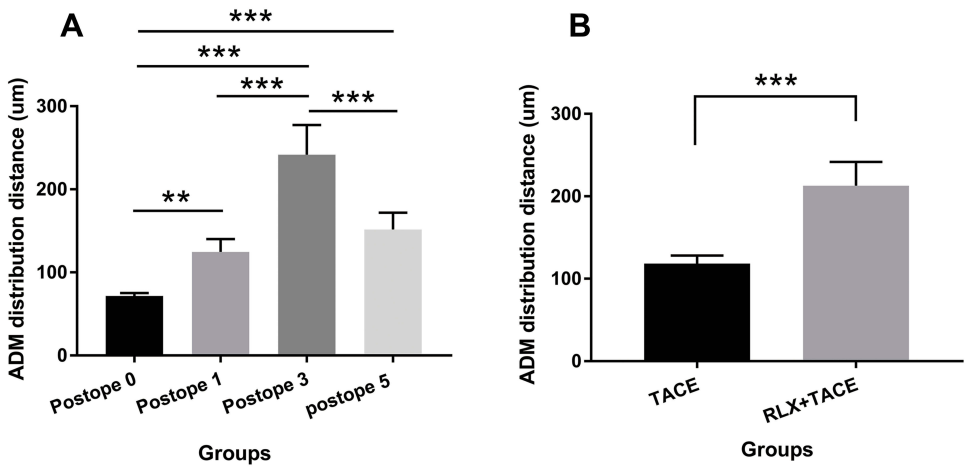

Figure 3 Image analysis of immunofluorescence of ADM pervasion distance was performed to evaluate the pervasion distance of ADM within the tumor stroma in the first part of this study. ** *P* <0.01; *** *P* <0.001.
Abbreviation: ADM, adriamycin.

of these two groups were 118.40±9.71 μm and 212.88±28.74 μm, respectively, with significant difference (p=0.000).

The MVD of each group was presented in Table 1. No significant difference was observed among these four groups (p=0.118).

TUNEL, Ki67 and HE Staining

TUNEL and Ki67 staining were conducted to evaluate the therapeutic effects on the groups 7, 8 and 9. The ratios of necrotic cells in the NS, TACE and RLX combined with TACE group were 0.30±0.08, 0.53±0.14 and 0.78±0.08, respectively, as shown in Figure 4. The difference of these three groups was significant between each other (p<0.05). Besides, the similar results were achieved in the Ki67 staining, the ratios of proliferous cells in the three groups were 0.37±0.07, 0.29±0.04 and 0.20±0.04, respectively (p<0.05). As shown in Figure 4, it is illustrated that the rate of cancer cells at the proliferation stage in the RLX combined with TACE group was significantly lower compared to the TACE and the NS groups. Moreover, HE staining indicated similar results, as shown in Figure 5.

Table 1 MVD in Three Groups

Groups	MVD
	Mean±SD
RLX+TACE	83.57±6.814
TACE	97.46±9.045
NS	80.33±7.652
F value	2.564
P value	0.118

Tumor Growth, Necrosis Rates and Metastasis

The tumor growth rate and the necrosis rate were summarized in Tables 2 and 3. The growth rates at the 1st week in groups 7, 8 and 9 were 2.33±0.67, 1.74±0.16 and 1.24 ±0.21, respectively, with significant difference (p<0.05).

The necrosis rates were 0.37±0.13, 0.69±0.10 and 0.85 ±0.08 in NS, TACE and RLX combined with TACE groups, respectively, with significant difference (p<0.05).

Moreover, the intrahepatic metastasis was summarized in Table 4 and there was no significant difference among the three groups (p=0.273).

Discussion

It has been identified that RLX is able to increase the expression of MMP-9 when collagen is abnormally produced like what happens in the tumor lump,[31,32] consistent with the results in this study. Given that no study applied the RLX directly in liver cancer treatment, particularly in interventional field, in order to study the effect of RLX in liver cancer treatment, we randomly assigned some rabbits into 4 groups and measured the MMP-2 and the MMP-9 activities after NS and RLX transcatheter injection at the same day and 1, 3 and 5 days after injection, respectively, according to Brown et al and Perentes et al.[33,34] The activity of MMP-9 within the tumor tissues was upregulated after the RLX injection while the MMP-2 activity was undetectable. Furthermore, the MMP-9 activity on the 3rd day after transcatheter operation was significantly upregulated compared with NS group, while its activity on the 1st and 5th day after the operation was not evident. However, the zymography results revealed

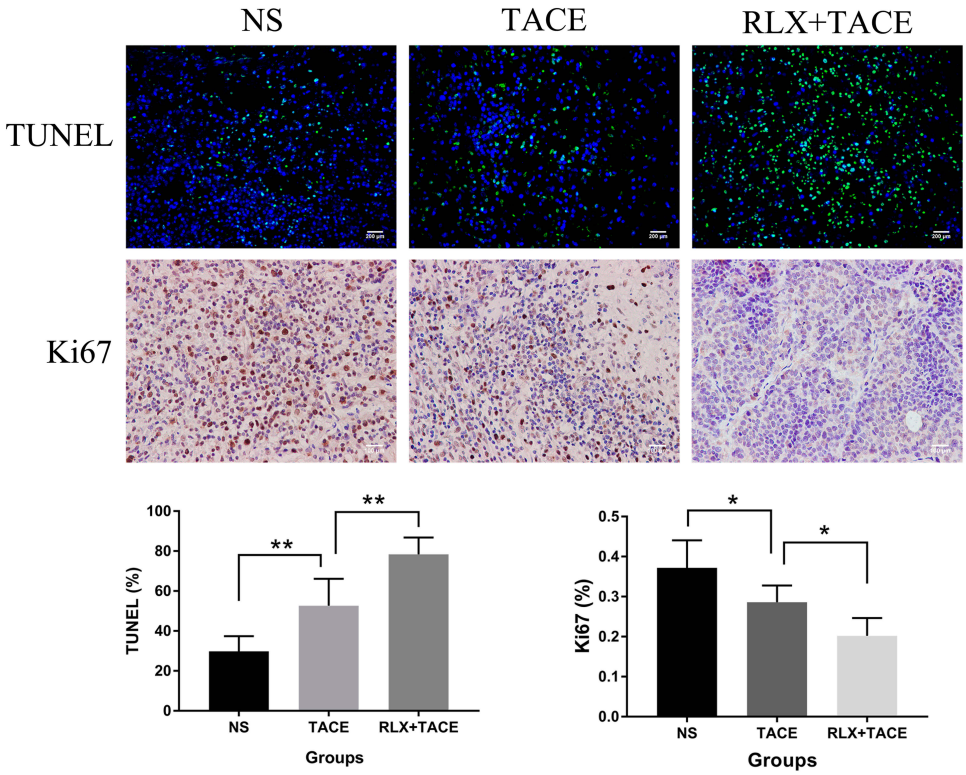

Figure 4 TUNEL and Ki67 staining were performed to evaluate the apoptosis and the proliferation of the harvested tumor tissues in groups 7, 8 and 9, respectively. *P<0.05; **P<0.01.

upregulated activity trends on the 1st and 5th day groups to some extent, compared with the operation day. Furthermore, it was further confirmed by the following ADM distribution analysis. To study whether TACE procedures would affect the MMPs activity after RLX injection through tumor feeding artery, the groups 5 and 6 were experimented, and the results demonstrated that RLX combined with TACE upregulated the MMP-9 activity significantly compared with the control group. Besides, the MMP-2 activity was undetectable.

In order to verify that hindrance of the ECM components in tumor tissues was degraded by increasing the MMP-9, the ADM distribution was investigated. As shown in Figures 1–3, the ADM distribution distance was in accordance with the MMP-9 activity, that means the more upregulation of the MMP-9 achieved, the farther the ADM reached. Therein the ADM in group 3 distributed significantly utmost, and the group 2 and 4 reached significantly farther than the group 1 as well. The results indicated that better intratumor infiltration was achieved by RLX injection through tumor feeding artery. Several researches have also acclaimed that the RLX can decrease the tumor ECM collagen, especially collagen I, and form porous structure. Thus, it can decrease the infiltration hindrance and subsequently allow that drug dispersed farther within the tumor.[26,27,29,34] This study not only verified the theoretical contribution of these researches, but also demonstrated that the transcatheter RLX injection was effective in destroying the ECM obstruction.

After destroying the physical barriers of the ECM, the therapeutic effects were then studied by transcatheter procedures, which have not been performed before as far as we know, but just Golubnitschaja et al reported that TACE treated patients tending to better survival in situation of lower MMP-9 activities.[35,36] ANOVA analysis revealed that the growth rate of the RLX combined with TACE group was significantly decreased compared with the TACE and the NS group, however, the necrosis rate was significantly increased compared with the other two groups. It indicated that RLX combined with TACE procedures for the treatment of VX2 tumor could result in impaired growth that complied with enhanced necrosis. Besides, the TUNEL and Ki67 staining identified the outcomes through cross-validation. Moreover, the HE staining also presented that a better effect was achieved in the RLX combined with TACE group.

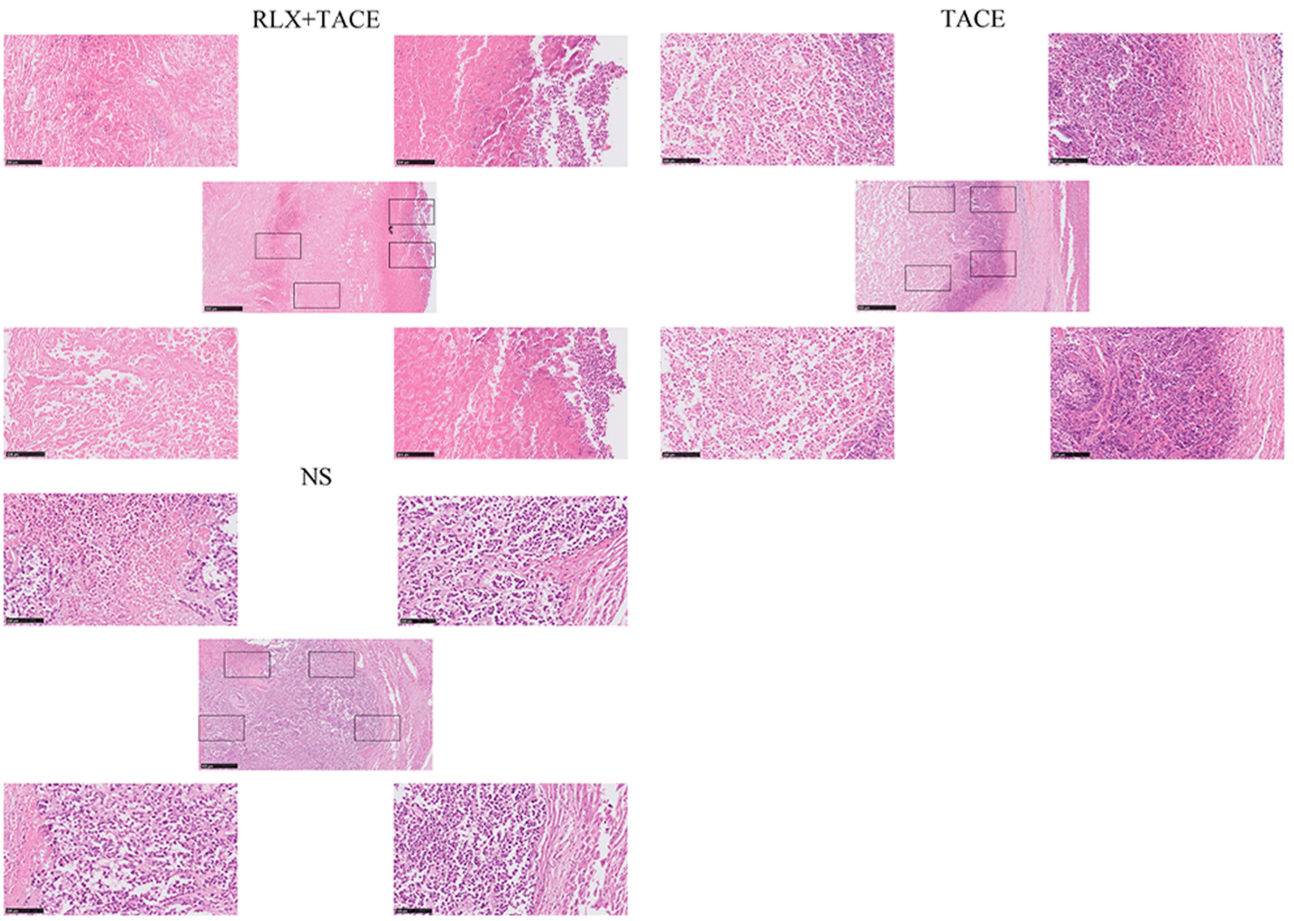

Figure 5 HE staining were performed to apoptosis of the harvested tumor tissues in groups 7, 8 and 9, respectively.

Given that ECM could obstruct drug penetration and interact with malignant cells,[8,13-15] the results attained in this study revealed that its degradation had a satisfactory lethal effect on VX2 tumor cells, however, the latter theory has not been studied here. Moreover, the inhibition of the tumor metastasis was further considered, since the previous researches have proved that the linearized ECM fiber provides a "highway" for cancer cells to invade blood vessels and around vessels, especially where it is coated with dense ECM.[16] However, although the metastasis nodules were fewer in the RLX combined with TACE group in the study, there was no significant difference among the three groups, which may be attributed to the limited observation time. Although some researches indicated that degraded ECM facilitates the tumor migration,[24,32] the general consensus is that the RLX does not induce metastasis, but reverses the spread of tumor cells.[8] Silvertown et al reported that RLX overexpression increased prostate xenograft tumor growth and angiogenesis, but it was reversed later by the same group.[32,37] However, the results in present study did not show any evidence that RLX could promote metastasis.

Table 2 The Tumor Growth Rate of Three Groups

Groups	Tumor Volume (cm^3)		Growth Rate
	V1 (Preoperation)	V2 (Postoperation)	V2/V1×100%
RLX+TACE	1.7±1.1	2.1±1.4	124.2±21.5
TACE	1.8±0.7	2.8±1.1	174.3±15.9
NS	1.8±0.2	3.4±0.5	233.3±67.3
F value			13.463
P value			0.000

Table 3 The Tumor Necrosis Rate of Three Groups

Groups	Tumor Necrosis Areas (cm^2)		Necrosis Rate
	S1	S2	S2/S1×100%
RLX+TACE	3.3±2.0	2.7±1.4	85.2±7.5
TACE	5.2±1.0	3.6±0.6	68.8±10.4
NS	5.3±1.4	1.9±0.7	37.4±13.2
F value			26.168
P value			0.001

Table 4 Number of the Intrahepatic Metastasis

Groups	Num. of Metastasis
	Mean
RLX+TACE	1.8
TACE	2.0
NS	2.8
F value	1.448
P value	0.273

Although TACE could destroy cancer cells ideally by starving it due to the embolization of supply arteries combined with poisoning it by chemotherapeutic drugs, the latter was hard to achieved for the guard of ECM. This study demonstrated that the RLX injection combined with TACE could destroy the hindrance of ECM and further improved therapeutic effect, thus providing new strategy for clinically benefitting HCC patients.

There were several limitations in this study. First, the sample size was small. Second, studied MMPs activity was confined to MMP-2 and MMP-9 due to the limited experimental technology, while MMP-3 may be also upregulated which was hinted by previous research.[23] Third, the dose of RLX and the time points of 0, 1, 3 and 5 days after RLX transcatheter injection were referred to previous researches.[33,34] Since the RLX acts in a dynamic process, more measurement time points about the MMP activity could provide additional information about its effect within tumor tissues. Fourth, which kinds of collagen was affected in the ECM components and further, how the interaction between cancer cells with the ECM changed were not included in the study.

In conclusion, this research for the first time used transcatheter RLX injection combined with TACE to improve drug penetration for the treatment of liver cancer. Furthermore, the MMP-9 activity was upregulated and the drug distribution was then enhanced after transcatheter RLX injection. Moreover, better outcomes were achieved due to increased necrosis rates and decreased growth rates after the combined use of RLX and TACE.

Acknowledgments

We are grateful to the Animal Center, the Department of Central Laboratory of Wuhan Union Hospital, Tongji Medical College, Huazhong University of Science and Technology.

Disclosure

The authors report no conflicts of interest in this work. The study was financially supported by grants from the National Natural Science Foundation of China (grant No. 81601580).

References

1. Bray F, Ferlay J, Soerjomataram I, et al. Global cancer statistics 2018: GLOBOCAN estimates of incidence and mortality worldwide for 36 cancers in 185 countries. *CA Cancer J Clin*. 2018;68(6):394–424. doi:10.3322/caac.21492
2. Llovet JM, Real MI, Montana X, et al. Arterial embolisation or chemoembolisation versus symptomatic treatment in patients with unresectable hepatocellular carcinoma: a randomised controlled trial. *Lancet*. 2002;359(9319):1734–1739. doi:10.1016/S0140-6736(02)08649-X
3. Lo CM, Ngan H, Tso WK, et al. Randomized controlled trial of transarterial lipiodol chemoembolization for unresectable hepatocellular carcinoma. *Hepatology*. 2002;35(5):1164–1171. doi:10.1053/jhep.2002.33156
4. Malagari K, Pomoni M, Moschouris H, et al. Chemoembolization with doxorubicin-eluting beads for unresectable hepatocellular carcinoma: five-year survival analysis. *Cardiovasc Intervent Radiol*. 2012;35(5):1119–1128. doi:10.1007/s00270-012-0394-0
5. Park J-W, Sherman M, Colombo M, et al. Observations of hepatocellular carcinoma (hcc) management patterns from the global hcc bridge study: first characterization of the full study population. *J Clin Oncol*. 2012;30(15_suppl):4033. doi:10.1200/jco.2012.30.15_suppl.4033
6. Takayasu K, Arii S, Kudo M, et al. Superselective transarterial chemoembolization for hepatocellular carcinoma. Validation of treatment algorithm proposed by japanese guidelines. *J Hepatol*. 2012;56(4):886–892. doi:10.1016/j.jhep.2011.10.021
7. Chang JM, Tzeng WS, Pan HB, et al. Transcatheter arterial embolization with or without cisplatin treatment of hepatocellular carcinoma. A randomized controlled study. *Cancer*. 1994;74(9):2449–2453. doi:10.1002/1097-0142(19941101)74:9<2449::AID-CNCR2820740910>3.0.CO;2-4
8. Egeblad M, Rasch MG, Weaver VM. Dynamic interplay between the collagen scaffold and tumor evolution. *Curr Opin Cell Biol*. 2010;22(5):697–706. doi:10.1016/j.ceb.2010.08.015
9. Choi IK, Strauss R, Richter M, et al. Strategies to increase drug penetration in solid tumors. *Front Oncol*. 2013;3:193. doi:10.3389/fonc.2013.00193
10. Bissell MJ, Radisky D. Putting tumours in context. *Nat Rev Cancer*. 2001;1(1):46–54. doi:10.1038/35094059
11. Mueller MM, Fusenig NE. Friends or foes - bipolar effects of the tumour stroma in cancer. *Nat Rev Cancer*. 2004;4(11):839–849. doi:10.1038/nrc1477
12. Bhowmick NA, Neilson EG, Moses HL. Stromal fibroblasts in cancer initiation and progression. *Nature*. 2004;432(7015):332–337. doi:10.1038/nature03096
13. Pylayeva Y, Gillen KM, Gerald W, et al. Ras- and pi3k-dependent breast tumorigenesis in mice and humans requires focal adhesion kinase signaling. *J Clin Invest*. 2009;119(2):252–266. doi:10.1172/JCI37160
14. Schrader J, Gordon-Walker TT, Aucott RL, et al. Matrix stiffness modulates proliferation, chemotherapeutic response, and dormancy in hepatocellular carcinoma cells. *Hepatology*. 2011;53(4):1192–1205. doi:10.1002/hep.24108
15. Erler JT, Bennewith KL, Cox TR, et al. Hypoxia-induced lysyl oxidase is a critical mediator of bone marrow cell recruitment to form the premetastatic niche. *Cancer Cell*. 2009;15(1):35–44. doi:10.1016/j.ccr.2008.11.012

16. Condeelis J, Segall JE. Intravital imaging of cell movement in tumours. *Nat Rev Cancer*. 2003;3(12):921–930. doi:10.1038/nrc1231
17. Desgrosellier JS, Cheresh DA. Integrins in cancer: biological implications and therapeutic opportunities. *Nat Rev Cancer*. 2010;10(1):9–22. doi:10.1038/nrc2748
18. Tlsty TD, Coussens LM. Tumor stroma and regulation of cancer development. *Annu Rev Pathol*. 2006;1:119–150. doi:10.1146/annurev.pathol.1.110304.100224
19. Dougan SK. The pancreatic cancer microenvironment. *Cancer J*. 2017;23(6):321–325. doi:10.1097/PPO.0000000000000288
20. Yun CO. Overcoming the extracellular matrix barrier to improve intratumoral spread and therapeutic potential of oncolytic virotherapy. *Curr Opin Mol Ther*. 2008;10(4):356–361.
21. Liang B, Chen S, Li L, et al. Effect of transcatheter intra-arterial therapies on tumor interstitial fluid pressure and its relation to drug penetration in a rabbit liver tumor model. *J Vasc Interv Radiol*. 2015;26(12):1879–1886. doi:10.1016/j.jvir.2015.05.031
22. Liang B, Xiong F, Wu H, et al. Effect of transcatheter intraarterial therapies on the distribution of doxorubicin in liver cancer in a rabbit model. *PLoS One*. 2013;8(10):e76388. doi:10.1371/journal.pone.0076388
23. Van Der Westhuizen ET, Summers RJ, Halls ML, et al. Relaxin receptors–new drug targets for multiple disease states. *Curr Drug Targets*. 2007;8(1):91–104. doi:10.2174/138945007779315650
24. Binder C, Hagemann T, Husen B, et al. Relaxin enhances in-vitro invasiveness of breast cancer cell lines by up-regulation of matrix metalloproteases. *Mol Hum Reprod*. 2002;8(9):789–796. doi:10.1093/molehr/8.9.789
25. Amento EP, Bhan AK, McCullagh KG, et al. Influences of gamma interferon on synovial fibroblast-like cells. Ia induction and inhibition of collagen synthesis. *J Clin Invest*. 1985;76(2):837–848. doi:10.1172/JCI112041
26. Cernaro V, Lacquaniti A, Lupica R, et al. Relaxin: new pathophysiological aspects and pharmacological perspectives for an old protein. *Med Res Rev*. 2014;34(1):77–105. doi:10.1002/med.21277
27. Beyer I, Li Z, Persson J, et al. Controlled extracellular matrix degradation in breast cancer tumors improves therapy by trastuzumab. *Mol Ther*. 2011;19(3):479–489. doi:10.1038/mt.2010.256
28. Hallden G, Portella G. Oncolytic virotherapy with modified adenoviruses and novel therapeutic targets. *Expert Opin Ther Targets*. 2012;16(10):945–958. doi:10.1517/14728222.2012.712962
29. Kim JH, Lee YS, Kim H, et al. Relaxin expression from tumor-targeting adenoviruses and its intratumoral spread, apoptosis induction, and efficacy. *J Natl Cancer Inst*. 2006;98(20):1482–1493. doi:10.1093/jnci/djj397
30. Weidner N, Semple JP, Welch WR, et al. Tumor angiogenesis and metastasis–correlation in invasive breast carcinoma. *N Engl J Med*. 1991;324(1):1–8. doi:10.1056/NEJM199101033240101
31. Williams EJ, Benyon RC, Trim N, et al. Relaxin inhibits effective collagen deposition by cultured hepatic stellate cells and decreases rat liver fibrosis in vivo. *Gut*. 2001;49(4):577–583. doi:10.1136/gut.49.4.577
32. Silvertown JD, Ng J, Sato T, et al. H2 relaxin overexpression increases in vivo prostate xenograft tumor growth and angiogenesis. *Int J Cancer*. 2006;118(1):62–73. doi:10.1002/ijc.21288
33. Brown E, McKee T, diTomaso E, et al. Dynamic imaging of collagen and its modulation in tumors in vivo using second-harmonic generation. *Nat Med*. 2003;9(6):796–800. doi:10.1038/nm879
34. Perentes JY, McKee TD, Ley CD, et al. In vivo imaging of extracellular matrix remodeling by tumor-associated fibroblasts. *Nat Methods*. 2009;6(2):143–145. doi:10.1038/nmeth.1295
35. Golubnitschaja O, Yeghiazaryan K, Stricker H, et al. Patients with hepatic breast cancer metastases demonstrate highly specific profiles of matrix metalloproteinases MMP-2 and MMP-9 after SIRT treatment as compared to other primary and secondary liver tumours. *BMC Cancer*. 2016;16:357. doi:10.1186/s12885-016-2382-2
36. Golubnitschaja O, Sridhar KC. Liver metastatic disease: new concepts and biomarker panels to improve individual outcomes. *Clin Exp Metastasis*. 2016;33(8):743–755. doi:10.1007/s10585-016-9816-8
37. Silvertown JD, Symes JC, Neschadim A, et al. Analog of h2 relaxin exhibits antagonistic properties and impairs prostate tumor growth. *FASEB J*. 2007;21(3):754–765. doi:10.1096/fj.06-6847com